IOP PUBLISHING INVERSE PROBLEMS

Inverse Problems **23** (2007) S11–S20 doi:10.1088/0266-5611/23/6/S02

# A series solution and a fast algorithm for the inversion of the spherical mean Radon transform

**Leonid A Kunyansky**

Department of Mathematics, University of Arizona, Tucson, AZ 85721, USA

E-mail: leonk@math.arizona.edu

Received 26 January 2007, in final form 5 April 2007
Published 23 November 2007
Online at stacks.iop.org/IP/23/S11

**Abstract**

An explicit series solution is proposed for the inversion of the spherical mean Radon transform. Such an inversion is required in problems of thermo- and photo-acoustic tomography. Closed-form inversion formulae are currently known only for the case when the centres of the integration spheres lie on a sphere surrounding the support of the unknown function, or on certain unbounded surfaces. Our approach results in an explicit series solution for any closed measuring surface surrounding a region for which the eigenfunctions of the Dirichlet Laplacian are explicitly known—such as, for example, cube, finite cylinder, half-sphere etc. In addition, we present a fast reconstruction algorithm applicable in the case when the detectors (the centres of the integration spheres) lie on a surface of a cube. This algorithm reconstructs 3D images thousands times faster than backprojection-type methods.

## 1. Introduction

The problem of image reconstruction in thermo-acoustic and photo-acoustic tomography is equivalent to recovering a function from a certain set of its spherical means [11, 13, 14, 18, 19]. The process starts with the object of interest being excited by a short electromagnetic pulse. This causes thermal expansion of the tissue, and generates an acoustic wave whose intensity is recorded by a set of detectors located outside the object. The intensity of the thermal expansion depends on the local properties of the tissue, and is of interest to a doctor, since abnormally high values of this function are indicative of a tumour. Under certain simplifying assumptions, the measurements can be related to the integrals of the expansion intensity over the spheres with the centres at the detectors' locations. The reconstruction of the local properties from these integrals is equivalent to the inversion of the spherical mean Radon transform.

Some of the recent results on the injectivity of this transform as well as the corresponding range conditions can be found in [1–4, 8, 9]. In the present paper we concentrate on inversion formulae and algorithms for the solution of the reconstruction problem. Generally,

 © 2007 IOP Publishing Ltd Printed in the UK 

in such applications as photo- and thermo-acoustic tomography, the designer of the measuring system has a certain freedom of choice when selecting the detectors' positions (the centres of the integration spheres). Most of the known explicit solutions pertain to the spherical acquisition geometry, in other words to the configuration in which the detectors are located on a sphere surrounding the object. Such are the recently found series solutions [16–18] and backprojection-type formulae [8, 10, 12, 19]. Explicit reconstruction formulae are also known for such acquisition geometries as an infinite plane [7, 15, 19] and an infinite cylinder [19].

The spherical geometry is preferable to unbounded measuring surfaces since the latter have to be truncated in practice, which leads to errors in the reconstruction. However, there are compelling reasons to consider other non-spherical bounded measuring surfaces as well. For example, as shown in section 3, if the detectors are located on a surface of a cube surrounding the object of investigation, it is possible to design a fast algorithm that reconstructs the unknown 3D function in a matter of seconds—as opposed to the several hours required for algorithms based on straightforward discretization of one of the 3D backprojection-type inversion formulae [8, 12, 19].

We thus present a series solution for the inversion of spherical mean Radon transform in the case when the centres of the integration spheres lie on a closed surface surrounding a bounded connected region in $\mathbb{R}^n$, $n \geqslant 2$. Our procedure requires knowledge of the eigenfunctions of the Dirichlet Laplacian defined on the region enclosed by the measuring surface. For many regions of practical interest such eigenfunctions are known explicitly. Among such regions in 3D are, for example, a cube, a ball, an ellipsoid, a cylinder, a spherical shell. In addition, these eigenfunctions can be easily found for certain subsets of these bodies obtained by dissecting them along a plane of symmetry—for example for a half-ball, half-cylinder, certain triangular prisms and tetrahedra. Yet another example of regions with explicitly known eigenfunctions is given by the crystallographic domains (see [5, 6] for details). A generalization of this approach to a general connected region is possible if one computes the eigenfunctions of the Dirichlet Laplacian numerically. In this case, however, the reconstruction algorithm is likely to be rather expensive from the computational point of view.

The proof of the range theorem in [1] involves implicitly a reconstruction procedure also based on eigenfunction expansions. Unlike the present method, that procedure would involve division of analytic functions that have a countable number of zeros. While the range theorem guarantees cancellation of these zeros when the data are in the range of the direct transform, a stable numerical implementation of such division would be complicated if not impossible. (A similar problem arises with the series solution of [16] that involves division of certain computed quantities by Bessel functions.) The technique we present below does not require such divisions.

Section 2 contains a general description of the present method. The efficiency of numerical realization of this technique depends, in particular, on the availability of fast algorithms for the summation of the arising eigenfunction expansions. In the simplest case of a cubic measuring surface (or a surface of a rectangular parallelepiped) such an algorithm is the 3D fast sine Fourier transform. This allows us to design a very efficient reconstruction algorithm for this particular measuring configuration, as discussed in section 3. Finally, in section 4 we investigate an interesting property that seems to be exclusive to the series solutions presented in this paper. Namely, this technique will produce a theoretically exact image within the region enclosed by the measuring surface even if there are sources outside that region. This property can prove to be useful for reducing the sensitivity of the measuring system to external noise. Such a noise cancellation will occur, however, only if all the measurements are performed simultaneously by a fixed set of detectors; a synthesized measuring surface will not exhibit this phenomenon.

## 2. Series solution

Suppose that the $C_0^1$ function $f(\mathbf{x}), \mathbf{x} \in \mathbb{R}^n, n \geqslant 2$ is compactly supported within the bounded connected open region $\Omega$ with boundary $\partial\Omega$. Our goal is to reconstruct $f(\mathbf{x})$ from its projections $g(\mathbf{z}, r)$ defined as the integrals of $f(\mathbf{x})$ over the spheres of radius $r$ centred at $\mathbf{z}$:

$$g(\mathbf{z}, r) = \int_{\mathbb{S}^{n-1}} f(\mathbf{z} + r\hat{t}) r^{n-1} \, \mathrm{d}s(\hat{t}),$$

where $\mathbb{S}^{n-1}$ is the unit sphere in $\mathbb{R}^n$, $\hat{t}$ is a unit vector, and $\mathrm{d}s$ is the normalized measure in $\mathbb{R}^n$. Projections are assumed to be known for all $\mathbf{z} \in \partial\Omega, 0 \leqslant r \leqslant \operatorname{diam}(\Omega)$ (integrals for $r > \operatorname{diam}(\Omega)$ automatically equal zero, since the corresponding integration spheres do not intersect the support of the function).

Suppose $\lambda_m^2, u_m(\mathbf{x})$ are the eigenvalues and normalized eigenfunctions of the Dirichlet Laplacian $-\Delta$ on $\Omega$ with zero boundary conditions, i.e.

$$\begin{aligned} &\Delta u_m(\mathbf{x}) + \lambda_m^2 u_m(\mathbf{x}) = 0, \qquad \mathbf{x} \in \Omega, \quad \Omega \subseteq \mathbb{R}^n, \\ &u_m(\mathbf{x}) = 0, \qquad \mathbf{x} \in \partial\Omega, \\ &\|u_m\|_2^2 \equiv \int_\Omega |u_m(\mathbf{x})|^2 \, \mathrm{d}\mathbf{x} = 1. \end{aligned} \tag{1}$$

We notice that $u_m(\mathbf{x})$ is the solution of the Dirichlet problem for the Helmholtz equation with zero boundary conditions and the wave number $\lambda_m$, and thus it admits the Helmholtz representation

$$u_m(\mathbf{x}) = \int_{\partial\Omega} \Phi_{\lambda_m}(|\mathbf{x} - \mathbf{z}|) \frac{\partial}{\partial \mathbf{n}} u_m(\mathbf{z}) \, \mathrm{d}s(\mathbf{z}) \qquad \mathbf{x} \in \Omega, \tag{2}$$

where $\Phi_{\lambda_m}(|\mathbf{x} - \mathbf{z}|)$ is a free-space rotationally invariant Green's function of the Helmholtz equation (1).

Our approach is based on the fact that eigenfunctions $\{u_m(\mathbf{x})\}_0^\infty$ form an orthonormal basis in $L_2(\Omega)$. Therefore $f(\mathbf{x})$ can be represented by the series

$$f(\mathbf{x}) = \sum_{m=0}^{\infty} \alpha_m u_m(\mathbf{x}) \tag{3}$$

with

$$\alpha_m = \int_\Omega u_m(\mathbf{x}) f(\mathbf{x}) \, \mathrm{d}\mathbf{x}. \tag{4}$$

Since $f(\mathbf{x})$ is $C_0^1$, series (3) converges pointwise. The reconstruction formula will result if we substitute representation (2) into (4) and interchange the order of integrations

$$\begin{aligned} \alpha_m &= \int_\Omega u_m(\mathbf{x}) f(\mathbf{x}) \, \mathrm{d}\mathbf{x} \\ &= \int_\Omega \left( \int_{\partial\Omega} \Phi_{\lambda_m}(|\mathbf{x} - \mathbf{z}|) \frac{\partial}{\partial \mathbf{n}} u_m(\mathbf{z}) \, \mathrm{d}s(\mathbf{z}) \right) f(\mathbf{x}) \, \mathrm{d}\mathbf{x} \\ &= \int_{\partial\Omega} \left( \int_\Omega \Phi_{\lambda_m}(|\mathbf{x} - \mathbf{z}|) f(\mathbf{x}) \, \mathrm{d}\mathbf{x} \right) \frac{\partial}{\partial \mathbf{n}} u_m(\mathbf{z}) \, \mathrm{d}s(\mathbf{z}) \qquad (5) \\ &= \int_{\partial\Omega} I(\mathbf{z}, \lambda_m) \frac{\partial}{\partial \mathbf{n}} u_m(\mathbf{z}) \, \mathrm{d}s(\mathbf{z}), \qquad (6) \end{aligned}$$

where

$$I(\mathbf{z}, \lambda_m) = \int_\Omega \Phi_{\lambda_m}(|\mathbf{x}-\mathbf{z}|) f(\mathbf{x})\, d\mathbf{x}.$$

The change of the integration order is justified by the continuity of eigenfunctions $u_m(\mathbf{x})$. Function $I(\mathbf{z}, \lambda_m)$ is easily computed from the projections

$$I(\mathbf{z}, \lambda_m) = \int_\Omega \Phi_{\lambda_m}(|\mathbf{x}-\mathbf{z}|) f(\mathbf{x})\, d\mathbf{x} = \int_{\mathbb{R}^+} g(\mathbf{z}, r)\Phi_{\lambda_m}(r)\, dr,$$

and with Fourier coefficients $\alpha_m$ now known, $f(\mathbf{x})$ is reconstructed by summing series (3).

If desired, this solution can be rewritten in the form of a backprojection-type formula:

$$\begin{aligned} f(\mathbf{x}) &= \sum_{m=0}^{\infty} \alpha_m u_m(\mathbf{x}) = \int_{\partial\Omega} \left( \sum_{m=0}^{\infty} \alpha_m \Phi_{\lambda_m}(|\mathbf{x}-\mathbf{z}|) \frac{\partial}{\partial \mathbf{n}} u_m(\mathbf{z}) \right) ds(\mathbf{z}) \\ &= \int_{\partial\Omega} h(\mathbf{z}, |\mathbf{x}-\mathbf{z}|)\, ds(\mathbf{z}), \end{aligned} \tag{7}$$

where

$$h(\mathbf{z}, t) = \sum_{m=0}^{\infty} \alpha_m \Phi_{\lambda_m}(t) \frac{\partial}{\partial \mathbf{n}} u_m(\mathbf{z}), \tag{8}$$

and coefficients $a_m$ are computed using equation (6). In the above formula, equation (7) is clearly a backprojection operator, and (8) is a filtration. However, the latter operator is now represented by a series rather than by a closed form expression. Moreover, this operator is not local in $\mathbf{z}$, unlike the filtration operator of the known closed-form explicit inversion formulae [8, 10, 12, 19].

Finally, we notice that if function $f(\mathbf{x})$ is not smooth but rather belongs to $L^2(\Omega)$, our reconstruction formulae are still valid if equation (3) is understood in the $L^2$ sense.

## 3. A fast algorithm for the cubic measurement surface in 3D

A cube is the simplest of the regions whose eigenfunctions of the Dirichlet Laplacian are known explicitly; they are products of sine functions. In the present section we exploit the simple structure of these eigenfunctions to develop a fast reconstruction algorithm applicable in the case when the detectors are located on a surface of a cube (a generalization to the case of a rectangular parallelepiped is straightforward). Such a measuring surface can be either sampled by regular detectors or synthesized from measurements made by interferometric line detectors as discussed in the introduction.

Let the sought function $f(\mathbf{x})$ be supported within the cube $\Omega = [0, R]\times[0, R]\times[0, R]$. We will index the normalized eigenfunctions $u_{\mathbf{m}}(\mathbf{x})$ and eigenvalues $\lambda_{\mathbf{m}}$ of the Dirichlet Laplacian on this region using vector $\mathbf{m} = (m_1, m_2, m_3)$, $m_1, m_2, m_3 \in \mathbb{N}$:

$$\begin{aligned} u_{\mathbf{m}}(\mathbf{x}) &= \frac{8}{R^3} \sin\frac{\pi m_1 x_1}{R} \sin\frac{\pi m_2 x_2}{R} \sin\frac{\pi m_3 x_3}{R}, \\ \lambda_{\mathbf{m}} &= \pi^2 |\mathbf{m}|^2 / R^2. \end{aligned}$$

Cube $\Omega$ has six faces $\delta\Omega_i$, $i = 1, \ldots, 6$:

$$\begin{aligned} \delta\Omega_1 &= \{\mathbf{x} | x_1 = R, 0 < x_2 < R, 0 < x_3 < R,\}, \\ \delta\Omega_2 &= \{\mathbf{x} | x_1 = 0, 0 < x_2 < R, 0 < x_3 < R,\}, \\ \delta\Omega_3 &= \{\mathbf{x} | x_2 = R, 0 < x_1 < R, 0 < x_3 < R,\}, \end{aligned}$$

$$\delta\Omega_4 = \{\mathbf{x} | x_2 = 0, 0 < x_1 < R, 0 < x_3 < R,\},$$
$$\delta\Omega_5 = \{\mathbf{x} | x_3 = R, 0 < x_1 < R, 0 < x_2 < R,\},$$
$$\delta\Omega_6 = \{\mathbf{x} | x_3 = 0, 0 < x_1 < R, 0 < x_2 < R,\}.$$

The values of the normal derivatives $\frac{\partial}{\partial \mathbf{n}} u_{\mathbf{m}}(\mathbf{x})$ of the eigenfunctions on the boundary are equal to certain products of sine functions:

$$\frac{\partial}{\partial \mathbf{n}} u_{\mathbf{m}}(\mathbf{x}) = \begin{cases} (-1)^{m_1} \dfrac{8\pi m_1}{R^4} \sin \dfrac{\pi m_2 x_2}{R} \sin \dfrac{\pi m_3 x_3}{R}, & \mathbf{x} \in \delta\Omega_1 \\ -\dfrac{8\pi m_1}{R^4} \sin \dfrac{\pi m_2 x_2}{R} \sin \dfrac{\pi m_3 x_3}{R}, & \mathbf{x} \in \delta\Omega_2 \\ (-1)^{m_2} \dfrac{8\pi m_2}{R^4} \sin \dfrac{\pi m_1 x_1}{R} \sin \dfrac{\pi m_3 x_3}{R}, & \mathbf{x} \in \delta\Omega_3 \\ -\dfrac{8\pi m_2}{R^4} \sin \dfrac{\pi m_1 x_1}{R} \sin \dfrac{\pi m_3 x_3}{R}, & \mathbf{x} \in \delta\Omega_4 \\ (-1)^{m_3} \dfrac{8\pi m_3}{R^4} \sin \dfrac{\pi m_1 x_1}{R} \sin \dfrac{\pi m_2 x_2}{R}, & \mathbf{x} \in \delta\Omega_5 \\ -\dfrac{8\pi m_3}{R^4} \sin \dfrac{\pi m_1 x_1}{R} \sin \dfrac{\pi m_2 x_2}{R}. & \mathbf{x} \in \delta\Omega_6. \end{cases} \tag{9}$$

As in section 2, in order to reconstruct $f(\mathbf{x})$ we recover Fourier coefficients $\alpha_{\mathbf{m}}$:

$$\begin{aligned} \alpha_{\mathbf{m}} &= \int_{\partial\Omega} I(\mathbf{z}, \lambda_{\mathbf{m}}) \frac{\partial}{\partial \mathbf{n}} u_{\mathbf{m}}(\mathbf{z}) \, \mathrm{d}s(\mathbf{z}) \\ &= \sum_{j=1}^{6} \int_{\partial\Omega_j} I(\mathbf{z}, \lambda_{\mathbf{m}}) \frac{\partial}{\partial \mathbf{n}} u_{\mathbf{m}}(\mathbf{z}) \, \mathrm{d}s(\mathbf{z}), \end{aligned} \tag{10}$$

where

$$I(\mathbf{z}, \lambda) = \int_0^{\sqrt{3}R} g(\mathbf{z}, r) \Phi_\lambda(r) \, \mathrm{d}r. \tag{11}$$

If we choose Green's function $\Phi_\lambda(t)$ in the form

$$\Phi_\lambda(t) = \frac{\cos \lambda t}{4\pi t},$$

equation (11) can be rewritten in the form of the cosine Fourier transform as follows:

$$I(\mathbf{z}, \lambda) = \frac{1}{4\pi} \int_0^{\sqrt{3}R} \left[ \frac{g(\mathbf{z}, r)}{r} \right] \cos \lambda r \, \mathrm{d}r. \tag{12}$$

As before, when coefficients $\alpha_{\mathbf{m}}$ have been found function $f(\mathbf{x})$ is obtained by summing the Fourier series

$$f(\mathbf{x}) = \sum_{\mathbf{m} \in \mathbb{N}^3} \alpha_{\mathbf{m}} u_{\mathbf{m}}(\mathbf{x}). \tag{13}$$

The above formulae are just a particular case of the inversion technique presented in the previous section. They yield theoretically exact reconstruction if the effects of discretization are neglected. However, in the practical computation only a limited range of frequencies $0 \leqslant \lambda \leqslant \lambda^{\text{Nyquist}}$ can be recovered from finitely sampled (in $r$) projections $g(\mathbf{z}, r)$ using equation (12). Therefore series (13) has to be truncated. The Gibbs phenomenon resulting from such a truncation can be reduced by application of a filter $\eta(\lambda_{\mathbf{m}})$, so that instead of the previous equation the following formula will be used to reconstruct an approximation to $f(\mathbf{x})$:

$$f(\mathbf{x}) \approx \sum_{\mathbf{m} \in \mathbb{N}^3, |\lambda_{\mathbf{m}}| \leqslant \lambda^{\text{Nyquist}}} \alpha_{\mathbf{m}} \eta(\lambda_{\mathbf{m}}) u_{\mathbf{m}}(\mathbf{x}). \tag{14}$$

The whole reconstruction procedure can be accelerated by utilizing the fast cosine Fourier transform to compute (12), the 3D fast sine Fourier transform to sum series (13), and the 2D fast sine transform to evaluate the six integrals in equation (10). However, there is one obstacle for implementing this plan. The integrals in (10) need to be computed for different values of $\lambda_{\mathbf{m}}$, and there are too many of these values to make the algorithm efficient. The workaround for this problem is to evaluate these integrals for a set of uniformly distributed values $\lambda_l = l\Delta\lambda, l = 0, 1, 2, \ldots$ and then to find the values needed for each of $\lambda_{\mathbf{m}}$ by interpolation. Such an interpolation in the spectral parameter $\lambda$ requires careful selection of discretization steps and interpolation techniques. The details of our implementation are presented below.

Suppose function $f(\mathbf{x})$ is to be reconstructed on the $n \times n \times n$ Cartesian grid, and the detectors are located at the nodes of 2D $n \times n$ Cartesian grids defined on the faces of the cube (values at the edges of the cube will not be needed). We will assume that the discretization step of measurements (in $r$) is approximately the same as the step of the Cartesian grids. Then the number of samples $n_1$ in one projection $g(\mathbf{z}, r)$ approximately equals $\sqrt{3}n$. Depending on a type of the fast cosine Fourier transform algorithm used to compute (12), the projections will have to be padded with zeros to make the total number of samples $n_2$ either a power of 2, or a product of small prime numbers. Thus, $n_1 \leqslant n_2 < 2n_1$. The Nyquist frequency $\lambda^{\text{Nyquist}}$ corresponding to such discretization equals $\pi(n_1 - 1)/D$, where diameter $D = \text{diam}(\Omega) = \sqrt{3}R$. With these parameters in mind we summarize the five steps of the fast reconstruction algorithm.

*Step 1*. The first step is to compute a discrete version of (11) using the fast (discrete) cosine Fourier transform of length $n_2$. This will produce values $I(\mathbf{z}, \lambda_l)$ for the frequencies $\lambda_l = l\lambda^{\text{Nyquist}}/(n_2 - 1), l = 0, 1, \ldots, n_2 - 1$. Importantly, as long as $n_1 \leqslant n_2$, the step of discretization of $I(\mathbf{z}, \lambda_l)$ in $\lambda$ is small enough to make it possible to approximately recover values of $I(\mathbf{z}, \lambda)$ (or a linear function of $I(\mathbf{z}, \lambda)$) for $\lambda \neq \lambda_l$ by interpolation.

*Step 2*. For each value of $\lambda_l$ compute integrals in the form

$$\int_{\partial\Omega_j} I(\mathbf{z}, \lambda_l) \sin\frac{\pi m_i x_i}{R} \sin\frac{\pi m_k x_k}{R}\, \mathrm{d}s(\mathbf{z}), \qquad j = 1, \ldots, 6, \tag{15}$$

for integer all integer $m_i, m_k$ by means of the 2D fast sine Fourier transform.

*Step 3*. Compute approximate values of integrals

$$\int_{\partial\Omega_j} I(\mathbf{z}, \lambda_{\mathbf{m}}) \sin\frac{\pi m_i x_i}{R} \sin\frac{\pi m_k x_k}{R}\, \mathrm{d}s(\mathbf{z}), \qquad j = 1, \ldots, 6,$$

by interpolating values obtained on step 2 (equation (15)). Some care should be taken to guarantee accuracy of computations on this step. It is well known that a low order interpolation in spectral parameter can lead to a suboptimal reconstruction, due to highly oscillatory nature of the Fourier transformant. An example and analysis of this phenomenon can be found in [15]. However, the Fourier transform of a finitely supported function is an analytic function of the spectral parameter, even if the function itself is known imprecisely. Therefore, higher order polynomial interpolation is applicable and does produce good results in this case. In our numerical experiments we observed that, indeed, the linear interpolation in $\lambda$ yields rather inaccurate reconstruction. The increase in the order of the polynomial interpolation significantly improves the image; if the 6th order Lagrange interpolation is utilized, the interpolation error is dominated by the discretization errors and further increase in the accuracy of interpolation is not needed.

(a) (b) (c)

**Figure 1.** Numerical example: (a) the phantom, (b) reconstruction from the exact data and (c) reconstruction from noisy data.

*Step 4*. Use values computed on step 3 to calculate $\lambda_{\mathbf{m}}$ by combining equations (9) and (10).

*Step 5*. Using the 3D fast Fourier sine transform to implement (14), compute values of $f(\mathbf{x})$ at the nodes of the 3D Cartesian grid.

A simple computation shows that the number of floating point operations implemented on each step of the algorithm is $\mathcal{O}(n^3 \log n)$ for steps 1, 2, and 5, and $\mathcal{O}(n^3)$ on steps 3 and 4, resulting in a total $\mathcal{O}(n^3 \log n)$ operation count for this technique. This has to be compared with $\mathcal{O}(n^5)$ operation count required by a backprojection step of a method resulting from a straightforward discretization of any of the explicit inversion formulae [8, 12, 19]. (The latter estimate assumes that the reconstruction is done on the $n \times n \times n$ Cartesian grid from $n^2$ detector positions.)

In what follows we present a numerical example illustrating the work of our algorithm. A function is reconstructed within the cube $[0, 1] \times [0, 1] \times [0, 1]$. The dimension of the grids were defined by the values of parameters $n = 129, n_1 = 223$ and $n_2 = 256$. As a filter we used the cosine window function

$$\eta(\lambda) = \begin{cases} \cos \dfrac{\pi\lambda}{2\lambda^{\text{Nyquist}}}, & \lambda \leqslant \lambda^{\text{Nyquist}}, \\ 0, & \lambda > \lambda^{\text{Nyquist}}. \end{cases}$$

We utilized the same phantom as in [12] to facilitate the comparison of the present results with the images reconstructed in the former work by application of discretized explicit inversion formulae. The phantom consists of eight characteristic functions of the balls with radii ranging from 0.06 to 0.13, whose centres lie in the plane $x_3 = 0$. The cross section of the phantom by the latter plane is shown in figure 1(a). Figure 1(b) shows the central cross section ($x_3 = 0$) of the reconstruction from the exact data.

In order to evaluate the sensitivity of the algorithm to noise in data, the imprecise measurements were modelled by adding to the projections normally distributed noise with the intensity 15% of the signal (in $L_2$-norm). In this experiment the values of the reconstructed function were set to zero outside of the cube $[0.05, 0.95] \times [0.05, 0.95] \times [0.05, 0.95]$, since the reconstruction from noisy data is unstable at the locations close to the detectors, due to the singular nature of Green's function. Such sensitivity is natural, and is an issue for other reconstruction techniques as well. For example, the slices of 3D images obtained in [12] were computed within the unit ball from the detectors located on a sphere of radius 1.1; the reconstruction in the close vicinity of the detectors was also avoided. The grey scale

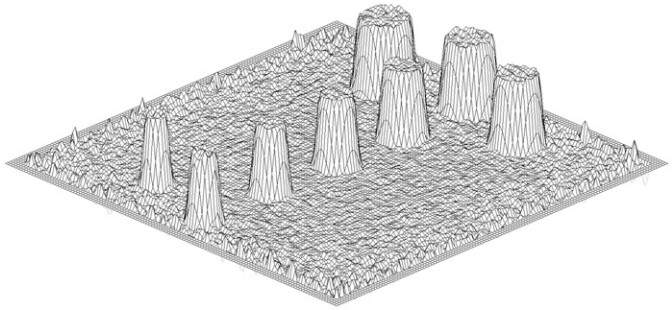

**Figure 2.** Reconstruction from noisy data; surface plot.

representation of the reconstructed function is shown in figure 1(c); in figure 2 we demonstrate the surface plot of the same function.

We believe that the quality of the reconstructed images in all of the above experiments is as good as of those resulting from explicit inversion formulae (see [12]). Similarly to those formulae the present technique demonstrates high stability of the algorithm to the perturbations of the data. On the other hand, the computation time for the present algorithm in the above experiment varied from 7 to 8 s on an AMD workstation with a 2 GHz processor; function values at about 2 million points were reconstructed from about 97 thousand projections. For comparison, the reconstruction reported in [12] from 33 000 projections at about a million grid points by the fastest of our implementations of the explicit inversion formula took about 48 min. If the latter algorithm is used to process the same number of the projections and grid points as in the present example (97 thousands and 2 million, respectively), the computation time increases to about 7 h. It is fair to say that the fast algorithm is thousands time faster than the straightforward discretization of any of the backprojection-type formulae.

## 4. Reconstruction in the presence of exterior sources

The series solution described above has an interesting property not possessed (to the best of our knowledge) by any other currently known explicit reconstruction technique. Let us consider a slightly more general problem. Suppose that region $\Omega$ is a proper subset of a larger region $\Omega_1$ ($\Omega \subset \Omega_1$) and that an $L^2$ function $F$ is defined on $\Omega_1$. In addition we will assume that $F(\mathbf{x}) = 0$ for all $\mathbf{x} \in \partial\Omega$. Let us denote the restriction of $F$ on $\Omega$ by $f$, i.e.

$$f(\mathbf{x}) = \begin{cases} F(\mathbf{x}), & \mathbf{x} \in \Omega, \\ 0, & \mathbf{x} \in \mathbb{R}^n \setminus \Omega. \end{cases}$$

We would like to reconstruct $f(\mathbf{x})$ from the integrals $g(\mathbf{z}, r)$ of $F$ over spheres with the centres on $\partial\Omega$:

$$g(\mathbf{z}, r) = \int_{\mathbb{S}^{n-1}} F(\mathbf{z} + r\hat{\mathbf{s}}) r^{n-1} \, d\hat{\mathbf{s}}, \qquad \mathbf{z} \in \partial\Omega.$$

Unlike in the previously considered problem, now the centres of the integration spheres are lying on a surface contained within the support $\Omega_1$ of the function $F$. While we are still trying to reconstruct the restriction $f$ of $F$ to $\Omega$, the integrals we know are those of $F$ and not of $f$.

It turns out that the solution to this problem is still given by formulae (3) and (6) (or equivalently by (7), (8) and (6)). Indeed, if we extend functions $u_m(\mathbf{x})$ by 0 to $\mathbb{R}^n$, formula (2) holds for all $\mathbf{x} \in \mathbb{R}^n$, and (3) remains unchanged. In formula (5) $f$ can be replaced by $F$ as

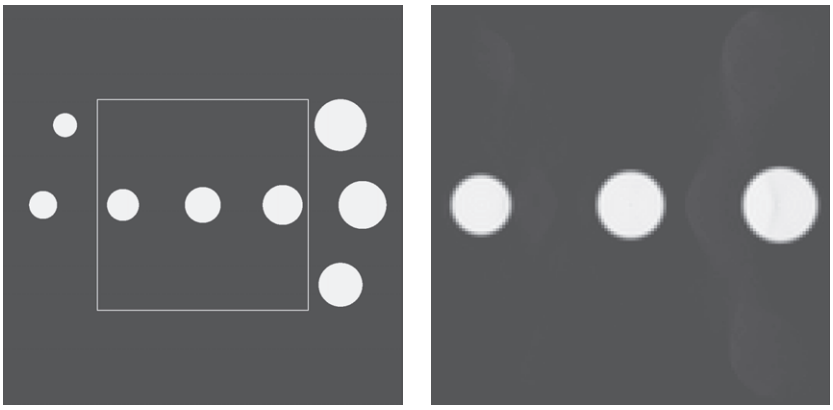

(a) (b)

**Figure 3.** Reconstruction in the presence of exterior sources (a) phantom; the white line shows location of the detectors (b) reconstructed image.

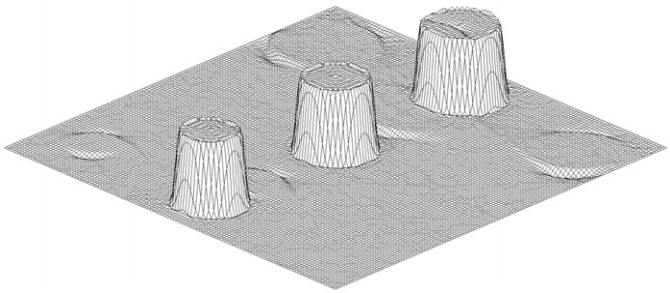

**Figure 4.** Reconstruction in the presence of exterior sources; surface plot.

follows:

$$\alpha_m = \int_\Omega u_m(\mathbf{x}) f(\mathbf{x})\,\mathrm{d}\mathbf{x} = \int_\Omega u_m(\mathbf{x}) F(\mathbf{x})\,\mathrm{d}\mathbf{x}$$
$$= \int_{\partial\Omega} \left( \int_\Omega \Phi_{\lambda_m}(|\mathbf{x}-\mathbf{z}|) F(\mathbf{x})\,\mathrm{d}\mathbf{x} \right) \frac{\partial}{\partial \mathbf{n}} u_m(\mathbf{z})\,\mathrm{d}s(\mathbf{z}),$$

and the inner integral can be computed from projections as before:

$$\int_\Omega \Phi_{\lambda_m}(|\mathbf{x}-\mathbf{z}|) F(\mathbf{x})\,\mathrm{d}\mathbf{x} = \int_{\mathbb{R}^+} g(\mathbf{z}, r)\Phi_{\lambda_m}(r)\,\mathrm{d}r.$$

By combining the two above equations we again arrive at the formula (6).

This interesting property can be illustrated by a numerical example. We consider the same phantom as in the previous section. This time, however, the detectors are located on the surface of the cube $\Omega = [0.235, 0.765] \times [0.235, 0.765] \times [0.235, 0.765]$. Location of the detectors is shown in figure 3(a) by a white line. The integrals were computed over full spheres, and the reconstruction was conducted, as before on the grid of size $129 \times 129 \times 129$ within $\Omega$. The result is presented in figure 3(b), and, as a surface plot, in figure 4. On the latter figure one can notice shallow troughs resulting from imperfect resolution of sharp edges of exterior sources by a finite number of detectors. The depths of these troughs, however, do not exceed 6% of the maximum of the original function.

## Acknowledgments

The author would like to thank P Kuchment for fruitful discussions and numerous helpful suggestions. We are also grateful to the anonymous referee for helpful comments and corrections. This work was partially supported by the NSF/DMS grant NSF-0312292 and by the DOE grant DE-FG02-03ER25577.

## References

[1] Agranovsky M, Kuchment P and Quinto E T 2006 Range descriptions for the spherical mean Radon transform *Preprint* math.AP/0606314
[2] Agranovsky M L and Quinto E T 1996 Injectivity sets for the Radon transform over circles and complete systems of radial functions *J. Funct. Anal.* **139** 383–414
[3] Ambartsoumian G and Kuchment P 2005 On the injectivity of the circular Radon transform arising in thermoacoustic tomography *Inverse Problems* **21** 473–85
[4] Ambartsoumian G and Kuchment P 2006 A range description for the planar circular Radon transform *SIAM J. Math. Anal.* **38** 681–92
[5] Bérard P 1979 Spectres et Groupes Cristallographiques *C. R. Acad. Sci. Paris A-B* **288** A1059–60
[6] Bérard P and Besson G 1980 Spectres et Groupes Cristallographiques II: Domaines Sphériques *Ann. Institut Fourier* **30** 237–48
[7] Fawcett J A 1985 Inversion of *N*-dimensional spherical averages *SIAM J. Appl. Math.* **45** 336–41
[8] Finch D, Patch S and Rakesh K 2004 Determining a function from its mean values over a family of spheres *SIAM J. Math. Anal.* **35** 1213–40
[9] Finch D and Rakesh 2006 The range of the spherical mean value operator for functions supported in a ball *Inverse Problems* **22** 923–38
[10] Finch D, Haltmeier M and Rakesh 2006 Inversion of spherical means and the wave equation in even dimensions *Preprint* math.AP/0701426
[11] Kuchment P 2006 Generalized transforms of radon type and their applications *The Radon Transform, Inverse Problems, and Tomography* ed G Olafsson and E T Quinto (*Proc. Symp. Appl. Math.* vol 63) (Providence, RI: American Mathematical Society) pp 67–91
[12] Kunyansky L A 2007 Explicit inversion formulae for the spherical mean Radon transform *Inverse Problems* **23** 373–83
[13] Kruger R A, Liu P, Fang Y R and Appledorn C R 1995 Photoacoustic ultrasound (PAUS) reconstruction tomography *Med. Phys.* **22** 1605–9
[14] Kruger R A, Reinecke D R and Kruger G A 1999 GA Thermoacoustic computed tomography—technical considerations *Med. Phys.* **26** 1832–7
[15] Natterer F and Wubbeling F 2001 Mathematical methods in image reconstruction *Monographs on Mathematical Modeling and Computation* vol 5 (Philadelphia, PA: SIAM)
[16] Norton S J 1980 Reconstruction of a two-dimensional reflecting medium over a circular domain: Exact solution *J. Acoust. Soc. Am.* **67** 1266–73
[17] Norton S J and Linzer M 1981 Ultrasonic reflectivity imaging in three dimensions—exact inverse scattering solutions for plane, cylindrical, and spherical apertures *IEEE Trans. Biomed. Eng.* **28** 202–20
[18] Xu M and Wang L-H V 2002 Time-domain reconstruction for thermoacoustic tomography in a spherical geometry *IEEE Trans. Med. Imag.* **21** 814–22
[19] Xu M and Wang L V 2005 Universal back-projection algorithm for photoacoustic computed tomography *Phys. Rev.* E **71** 016706